The Cryosphere Discuss., https://doi.org/10.5194/tc-2018-275
Manuscript under review for journal The Cryosphere
Discussion started: 20 February 2019

The Cryosphere Discussions
Open Access
EGU

Using a composite flow law to model deformation in the NEEM deep ice core, Greenland: Part 2 the role of grain size and premelting on ice deformation at high homologous temperature

Ernst-Jan N. Kuiper[1,2], Johannes H. P. de Bresser[1], Martyn R. Drury[1], Jan Eichler[2,3], Gill M. Pennock[1], Ilka Weikusat[2,1,3]

[1]Faculty of Earth Science, Utrecht University, 3508 TA Utrecht, the Netherlands
[2]Alfred Wegener Institute, Helmholtz Centre for Polar and Marine Research, 27570 Bremerhaven, Germany
[3]Department of Geosciences, Eberhard Karls University Tübingen, 72074 Tübingen, Germany

Correspondence to: E.N.Kuiper@uu.nl and Ilka.Weikusat@awi.de

Abstract. The ice microstructure in the lower part of the North Greenland Eemian Ice Drilling (NEEM) ice core consists of relatively fine grained glacial ice with a single maximum crystallographic preferred orientation (CPO) alternated by much coarser grained Eemian ice with a partial girdle type of CPO. In this study, the grain size sensitive (GSS) composite flow law of Goldsby and Kohlstedt (2001) was used to study the effects of grain size and premelting on strain rate in the lower part of the NEEM ice core. The results show that the strain rates predicted in the fine grained glacial layers are about an order of magnitude higher than in the much coarser grained Eemian layers. The dominant deformation mechanisms between the layers is also different with basal slip accommodated by grain boundary sliding (GBS-limited creep) being the dominant deformation mechanism in the glacial layers, while GBS-limited creep and dislocation creep (basal slip accommodated by non-basal slip) contribute both roughly equally to bulk strain in the coarse grained layers. Due to the large difference in microstructure between the impurity-rich glacial ice and the impurity-depleted Eemian ice at premelting temperatures (T>262K), it is expected that the fine grained layers deform mainly by simple shear at high strain rates, while the coarse grained layers are relatively stagnant. The difference in microstructure, and consequently in viscosity, between glacial and interglacial ice at temperatures just below the melting point can have important consequences for ice dynamics close to the bedrock.

1 Introduction

As a consequence of anthropogenic global warming, it is expected that global mean sea level (GMSL) rise will accelerate in the next decades and centuries (e.g. IPCC, 2014; Kopp et al., 2017). To improve the predictions in GMSL rise, the flow of ice in polar ice sheet models should be accurately described, since it is expected that the melting of the polar ice sheets will contribute significantly to future GMSL rise (IPCC, 2014). Therefore, a full understanding and description of ice deformation mechanisms in polar ice sheets is required. Ice in the lower part of polar ice sheets is of particular interest.

The Cryosphere Discuss., https://doi.org/10.5194/tc-2018-275
Manuscript under review for journal The Cryosphere
Discussion started: 20 February 2019

Generally, this ice is expected to deform much faster than the shallower ice, due to the well-developed crystallographic preferred orientation (CPO), relatively high temperatures near the bedrock and shear stress increase towards the bedrock. However, stress and strain rates near the bedrock can vary considerably due to the influence of bedrock variations, slippery patches or subglacial lakes (e.g. Budd and Rowden-rich, 1985; Gudlaugsson et al., 2016; Wolovick and Creyts, 2016). The high variation in deformation rates in the ice near the bedrock are often shown by borehole surveys (e.g. Gow and Williamson, 1976; Paterson, 1983; Thorsteinsson et al., 1999; Weikusat et al., 2017). The main source of heat of the ice near the bedrock is geothermal heat, which typically has a strength of 50-100 mW m^{-2} (Rogozhina et al., 2016). Locally, other sources of heat can be important, like shear heating (e.g. Krabbendam, 2016) or latent heat released by refreezing of melt water coming from the surface that drained into the interior of the ice sheet (e.g. Zwally et al., 2002; Van de Wal et al., 2008; Catania and Neumann, 2010).

Ice deformation experiments have shown that the effect of temperature on the strain rate of ice can be described via a calibrated Arrhenius type flow law relating equivalent strain rate to equivalent stress and temperature (e.g. Glen, 1955; Homer and Glen, 1978; Morgan, 1991). However, at temperatures close to the melting point, the strain rate increase has been found to be higher than predicted by the extrapolation of lower temperature results using the Arrhenius relation, inferred to be due to the initiation of a new high temperature deformation mechanism or to the enhancement of the orginal one. To account for the latter, a higher activation energy is often used above a certain temperature threshold (e.g., Mellor and Testa, 1969; Barnes et al., 1971; Paterson, 1994; Goldsby and Kohlstedt, 2001). This higher activation energy, which is the result of a simple best-fit approach of temperature and strain rate using a Arrhenius type relation, lacks a good link with the controlling deformation mechanism, assumed to be intracrystalline dislocation motion. Therefore, its application is not well founded. In experiments on ice single crystals and bicrystals close to the melting point (Homer and Glen, 1978; Jones and Brunet, 1978), a strong strain rate increase has not been observed. This strongly suggests that the strain rate enhancement in natural ice close to the melting point is related to the occurrence of grain boundaries.

Premelting along grain boundaries has often been stated as being responsible for the high strain rates during ice deformation tests at high temperatures (e.g. Mellor and Testa, 1969; Dash et al., 1995, 2006; Wilson et al., 1996; Wilson and Zhang, 1996). Premelting is expected to initiate at surfaces or interfaces such as grain boundaries where the crystallographic structure is disrupted and molecules can adopt water-like qualities at temperatures below the melting point (e.g. Orem and Adamson, 1969; Barnes et al., 1971; Dash et al., 1995, 2006; Döppenschmidt et al., 1998). High temperature deformation tests on polycrystalline ice have shown that a small liquid-like amorphous layer at the grain boundary increases grain boundary mobility by two to four orders of magnitudes (Duval and Castelnau, 1995; Schulson and Duval, 2009). Contrary to almost all other materials, grain boundary melting in ice at high cryostatic pressure is a thermodynamically favorable process as grain boundary melting causes a negative volume change of about 9% due to the low atomic packing factor of hexagonal ice (e.g. Schulson and Duval, 2009).

The different activation energy reflecting the onset of premelting is used widely at a temperature threshold of -10°C (263K) when applying Glen's flow law in ice sheet models (e.g. Paterson, 1994), but a higher temperature threshold of -8°C

(285K) (Barnes et al., 1971) or lower temperature thresholds of -15°C (258K) to -18°C (255K) (Goldsby and Kohlstedt, 2001) should be considered. As temperature generally increases with depth in polar ice sheets, the temperature where premelting starts to affect ice rheology is important. A low premelting temperature would mean that a considerable larger portion of the ice is affected by premelting, hence will show strain rate enhancement over a larger range, compared to a higher temperature threshold.

At temperatures close to the melting point in the lower part of polar ice cores, a particular type of microstructure with very coarse grains and interlocking grain boundaries is often found (e.g. Gow and Williams, 1976; Gow and Engelhardt, 2000; NEEM community members, 2013; Weikusat et al., 2017). In the lower part of the North Greenland Eemian Ice Drilling (NEEM) ice core such regions of coarse, interlocking grains are alternated by regions of finer grains (NEEM community members, 2013). In case of the NEEM ice core, the alternated layers of fine and coarse grained ice are the results of stratigraphic disruptions and overturned folds, which consist of impurity-rich glacial ice from the penultimate glacial period and impurity-depleted Eemian interglacial ice (NEEM community members, 2013).

These coarse grained layers at the bottom of some polar ice cores typically possess CPOs that could be described as a multi maxima, although the exact type of CPO is often unclear due to the low number of grains measured in individual thin sections. The coarse grains and multi maxima CPO are thought to be the result of rapid strain induced boundary migration (SIBM) in combination with the nucleation of new grains (SIBM-N) (e.g. Alley, 1992; Duval and Castelnau, 1995; Durand et al., 2009; Faria et al., 2014). SIBM is the migration of grain boundaries driven by the difference in stored strain energy between neighbouring grains that result from lattice distortions such as dislocations (Humphreys and Hatherly, 2004). SIBM starts in firn (Kipfstuhl et al., 2006, 2009) and is assumed to increase grain size (e.g. Duval and Castelnau, 1995), although under certain conditions SIBM can also be a grain size reducing mechanism by grain dissection (Steinbach et al., 2017). The layers of alternating grain size in deeper NEEM samples allows for the study of the effect of premelting and grain size on strain rate and CPO development.

In this study, the composite flow law of Goldsby and Kohlstedt (2001) was used to explore the effect of grain size on strain rate in the lower part of the NEEM ice core. The composite flow law describes the deformation of polycrystalline ice as a combination of grain size sensitive (GSS) and grain size insensitive (GSI) deformation mechanisms, where the dominant deformation mechanism depends on the temperature, stress and grain size. Compared to the companion paper (part 1), which describes ice deformation at relatively low temperatures in the upper 2207 m of the NEEM ice core, the emphasis in this paper is on possible differences in the controlling deformation mechanism close to the melting point. The results from flow law calculations were combined with CPO data to study deformation mechanisms in the lower part of the NEEM ice core. The NEEM ice core was chosen because of the high density of reflective light microscopy (LM) images (Kipfstuhl, 2010; Binder et al., 2013) and the alternation of fine and coarse grained layers in the lower part of the ice core. These reflective LM images were used to determine the change in grain size with depth (Binder, 2014). Furthermore, the CPO data of the NEEM ice core (Eichler et al., 2013) were available. A critical assessment of the temperature threshold for the onset of premelting in polar ice sheets led to a modification of the composite flow law of Goldsby and Kohlstedt (2001). The NEEM

ice core data were used to calculate the strain rate predicted by Glen's flow law (Glen, 1952, 1955; Paterson, 1994) and by the modified composite flow law of Goldsby and Kohlstedt (2001) in the lower part of the NEEM ice core. Possible deformation mechanisms are discussed.

2 Methods

2.1 The NEEM ice core and ice microstructure data

The NEEM ice core, located in the northwest of Greenland (77.45°N, 51.06°W), was drilled during the field seasons of 2008-2012 (NEEM community members, 2013; Rasmussen et al., 2013). The NEEM ice core is 2540 m long with ice deposited during the Holocene (Holocene ice) extending till a depth of 1419 m (Montagnat et al., 2014). Ice deposited during the last glacial period (glacial ice) lies below reaching a depth of 2207 m. The layering below the glacial ice is strongly disturbed and four stratigraphic disruptions were identified at 2209.6 m, 2262.2 m, 2364.5 m and 2432.2 m of depth by discontinuities in oxygen stable isotope values ($\delta^{18}O_{ice}$) of H_2O and methane (CH_4) (NEEM community members, 2013). These folded and overturned parts are from the interface between the glacial ice and the Eemian ice, which causes the coarse grained Eemian ice to be alternated with the finer grained glacial ice in the lowest 330 m of depth in the NEEM ice core. In the remainder of this study, the ice from 2207 m of depth till the ice-bedrock interface at 2540 m of depth will be referred to as the 'Eemian-glacial facies'.

The lower part of the glacial ice of the NEEM ice core was included in this study to show the contrast in grain size, CPO and calculated strain rate between the glacial ice and the Eemian-glacial facies. Therefore, the available LM images, orientation images and CPO data below 2000 m of depth were included in this study. Calculations using the GSS composite flow law of Goldsby and Kohlstedt require grain size as an input variable. The grain size data in the lowest 540 m of the NEEM ice core were obtained using 224 large area scanning macroscope (LASM) images (Kipfstuhl, 2010) taken using reflective light macroscopy (Krischke et al., 2015). This method uses thermal etching by sublimation to reveal (sub)grain boundaries as grooves on the surface of the ice core sample (e.g. Saylor and Rohrer, 1999) and has a resolution of 5 µm per pixel edge. Each LASM image is about 90 mm long by about 55 mm wide (Kipfstuhl et al., 2006) and was digitally analyzed using the Ice-image software (www.ice-image.org) (Binder et al., 2013; Binder, 2014). The software automatically detects the grain area of each grain by counting the pixels enclosed by grain boundaries. The total area classified as 'grain' by the Ice-image software was divided by the number of grains and a mean grain diameter was calculated assuming circular grains. Deriving a full grain size distribution, as was done in the companion paper (part 1), was not possible in the Eemian-glacial facies because the number of grains in the LASM images (90 x 55 mm) of the coarse grained layers was too low. Grains with a diameter <0.3 mm were excluded from the data set as these grains are often artefacts caused by relaxation (Binder, 2014). In some parts of the Eemian-glacial facies, the grains grow up to several centimetres and the grain boundaries are irregular with many grain boundary bulges. It is not possible to determine a mean grain size for these ice core sections by the Ice-image software as these grains often cross the edge of the LM images and are therefore not included in the grain size data

The Cryosphere Discuss., https://doi.org/10.5194/tc-2018-275
Manuscript under review for journal The Cryosphere
Discussion started: 20 February 2019

(Binder, 2014). After visual inspection of the LASM images to check the grain size, the ice core sections containing very large grains were assigned a mean grain diameter of 30 mm, which was the estimated grain diameter based on the LASM images.

An automatic Fabric Analyzer (FA) was used to create high-resolution maps of the c-axes orientations. The method is based on the double-refracting properties of the hexagonal ice crystal. It offers a fast alternative for the measurement of crystal orientations, which are, however, limited only to the c-axes. The grains in each orientation image were plotted in a pole figure. For each orientation images the Woodcock parameter was calculated (Woodcock, 1977). The Woodcock parameter is often used in order to distinguish between cluster and girdle type of CPOs. A distribution with a Woodcock parameter >1 indicates a cluster, while a Woodcock parameter <1 indicates a girdle. Further computer-based analysis (Eichler et al., 2013) of the FA-CPO-maps enables the derivation of a variety of microstructural parameters, such as mean grain shape or size. These can be used as complementary values to the LASM analysis data. However, these microstructural parameters can differ significantly from the microstructural parameters obtained by the Ice-image software (www.ice-image.org) (Binder et al., 2013; Binder, 2014). For instance, the mean grain size derived from the orientation images in this study is systematically shifted towards lower values, which is mainly caused by the exclusion of grains with a grain diameter <0.3 mm in the LASM method as was described above. In the remainder of this paper, the grain size determined using the Ice-image software (Binder et al., 2013; Binder, 2014) will be used unless stated otherwise.

2.2 Flow laws and flow law parameters

One of the two flow laws that was used during this study is the composite flow law of Goldsby and Kohlstedt (2001). The composite flow law was derived during uniaxial deformation tests in secondary creep with very fine grained ice (Goldsby and Kohlstedt, 1997, 2001). The composite flow law combines different deformation mechanisms of ice explicitly, instead of presenting a series of individual flow laws. During their uniaxial deformation experiments on artificial fine grained ice in secondary creep, Goldsby and Kohlstedt (1997, 2001) found four different deformation regimes with the composite flow law formulated as follows:

$$\dot{\varepsilon} = \dot{\varepsilon}_{\mathrm{disl}} + \left(\frac{1}{\dot{\varepsilon}_{\mathrm{basal}}} + \frac{1}{\dot{\varepsilon}_{\mathrm{GBS}}}\right)^{-1} + \dot{\varepsilon}_{\mathrm{diff}}, \qquad (1)$$

where $\dot{\varepsilon}$ is the strain rate. $\dot{\varepsilon}_{\mathrm{disl}}$ refers to dislocation creep where basal slip is the main strain producing mechanism, accommodated (i.e. rate-limited) by non-basal slip and $\dot{\varepsilon}_{\mathrm{diff}}$ refers to diffusion creep. Basal slip and grain boundary sliding are sequential processes acting together, where the slower mechanism determines the overall strain rate by accommodating the faster mechanism (Durham and Stern, 2001). In the part in between brackets in equation (1), $\dot{\varepsilon}_{basal}$ refers to GBS accomodated by basal slip, while $\dot{\varepsilon}_{\mathrm{GBS}}$ represents basal slip accommodated by GBS. Under stress, grain size and temperature conditions appropriate for terrestrial ice, diffusion creep and grain boundary sliding accommodated by basal slip are not relevant for ice deformation (Goldsby and Kohlstedt, 2001; Goldsby, 2006). Therefore, the composite flow law simplifies to:

$$\dot{\varepsilon} = \dot{\varepsilon}_{disl} + \dot{\varepsilon}_{GBS}, \qquad (2)$$

The Cryosphere Discuss., https://doi.org/10.5194/tc-2018-275
Manuscript under review for journal The Cryosphere
Discussion started: 20 February 2019

The strain rate produced by creep can be described by the following general flow law:

$$\dot{\varepsilon} = A\,\sigma^{n}\,d^{-p}\exp\left(-\frac{Q}{R\,T}\right), \qquad (3)$$

where $\dot{\varepsilon}$ is the strain rate (s^{-1}), A is a material parameter, σ is the stress (MPa), n is the stress exponent (dimensionless), d is the grain size (m), p is the grain size exponent (dimensionless), Q is the activation energy (J mol^{-1}), R the gas constant (J K^{-1} mol^{-1}) and T the absolute temperature (K) corrected for the change in pressure-melting point due to the cryostatic pressure. The value for p determines whether the creep is grain size insensitive (p=0) or grain size sensitive (p≠0). The mean grain diameter, as determined from LASM images with the Ice-image software, was used for the calculation of the strain rate produced by GBS-limited creep.

If the temperature is expressed in terms of the difference with the pressure-melting point, ice can, as a first order approximation, be considered incompressible (Rigsby, 1958; Doake and Wolff, 1985). The pressure-melting temperature was calculated according to:

$$T_m = -C\,\Delta P, \qquad (4)$$

where T_m is the pressure-melting temperature (°C), C is the pressure-melting constant for glacier ice ($9.8\,10^{-8}$ °C Pa^{-1}; Lliboutry, 1976) and ΔP is the overburden pressure (Pa) which was calculated according to:

$$\Delta P = \rho_{ice}\,h_{ice}\,g, \qquad (5)$$

where ρ_{ice} is the density of ice (910 kg m^{-3}), h_{ice} is the ice thickness (m) and g is the gravitational constant (9.81 m s^{-2}). The in-situ temperature (T) profile of the NEEM ice core was taken from Sheldon et al. (2014). In the remainder of this paper, T^* is used for the difference in temperature of the ice at a certain depth with respect to the pressure-melting point at that depth, which can be calculated according to:

$$T^* = T - T_m. \qquad (6)$$

T^* was used in Equation (3) to calculate the strain rates in the lower part of the NEEM ice core according to Glen's flow law and the composite flow law. At the base of the 2540 m long NEEM ice core the pressure-melting point is calculated to be -2.2°C (271K). For example, the in-situ temperature at the ice-bedrock interface at NEEM is -3.4°C, which would give a T^* of -1.2°C (Equation 6).

The other flow law that was used in the this study is Glen's flow law (Glen, 1952, 1955; Paterson, 1994), which is the flow law that is commonly used in ice sheet modelling. Glen's flow law is based on the results of uniaxial compression experiments on artificial, (initially) isotropic polycrystalline ice. Glen's flow law has the same form as Equation (3), but is independent of grain size (i.e., p=0) and is characterized by a stress exponent of n=3 (Glen, 1955; Paterson, 1994). Following the analysis presented in the companion paper (part 1), a constant equivalent stress of 0.07 MPa was taken as input for Glen's flow law and the composite flow law.

The Cryosphere Discuss., https://doi.org/10.5194/tc-2018-275
Manuscript under review for journal The Cryosphere
Discussion started: 20 February 2019

3 Results

3.1 Ice microstructure in the Eemian-glacial facies

Figure 1 shows reflective LM images and orientation images with pole figures of three ice core sections at 2258 m, 2264 m, 2308 m of depth in the Eemian-glacial facies. The ice core section at 2258 m of depth in Figure 1a is from just above the stratigraphic disruption at 2262.2 m of depth, while the ice core section at 2264 m of depth in Figure 1b is from just below this stratigraphic disruption. The ice core section in Figure 1c is from 2308 m of depth in the middle of one of the overturned layers (NEEM community members, 2013). The ice core section in Figure 1a is one of the finer grained ice core sections in the Eemian-glacial facies with a mean grain size of about 5 mm and originates from the beginning of the last glacial period (NEEM community members, 2013). The orientation image and pole figure of Figure 1a show that, similar to the glacial ice (1419-2207 m of depth; Montagnat et al., 2014), almost all c-axes are strongly aligned parallel to the vertical ice core axis. However, compared to the glacial ice, the grain size of the ice core section in Figure 1a is slightly larger and the grain shape is more irregular. The ice core section in Figure 1b is one of the ice core sections that was given a mean grain size of 30 mm. This ice core section originates from the end of the Eemian period (NEEM community members, 2013). The grains have an irregular shape with many millimetre sized bulges along the grain boundaries. The orientation image and pole figure show that the c-axes are distributed in a partial girdle spanning about 40° from the vertical axis. The ice core section in Figure 1c has a mean grain size of about 7 mm and originates from the end of the Eemian period (NEEM community members, 2013). The grain boundaries are bulging and have an irregular shape. The orientation image and pole figure show that the c-axes are distributed in a partial girdle spanning about 30° to 40° from the vertical axis.

3.2 Correlation mean grain diameter with type and strength of CPO

The correlation between the mean grain diameter and the type and strength of CPO in the lowest 540 m of the NEEM ice core is shown in Figure 2. This figure shows the first c-axes eigenvalue (Eichler et al., 2013) and the Woodcock parameter (Woodcock, 1977) versus the mean grain diameter for each orientation image in the lower part of the glacial ice (2000-2207 m of depth) and the ice in the Eemian-glacial facies (2207-2540 m of depth). The ice from the lower part of the glacial period (2000-2207 m of depth), which has a finer mean grain diameter (about 2 mm) than the ice in the Eemian-glacial facies, has a c-axes eigenvalue of >0.9 and the Woodcock parameter typically varies from 4-10. Some of the finest grained regions in the Eemian-glacial facies have a slightly larger mean grain diameter (3-5 mm) with a similar c-axes eigenvalue of >0.9 and a rather similar Woodcock parameter of about 2-10. For ice core sections with a mean grain diameter larger than about 5 mm, the eigenvalue is <0.9 with a Woodcock parameter varying from 0.3-3. However, the number of grains per orientation image decreases with increasing grain size and therefore the statistical significance of the first eigenvalue and Woodcock parameter decreases with increasing mean grain diameter. Based on Figure 2, two classes of grains can be distinguished based on mean grain diameter and type and strength of CPO. The first class has a relatively fine mean grain

diameter of <5 mm that is comparable in eigenvalue and Woodcock parameter to the glacial ice (green rectangle). The other class has a mean grain diameter of >5 mm with a relatively low first eigenvalue and Woodcock parameter (yellow rectangle).

3.3 Transition temperature: NEEM results compared to other polar ice cores

Table 1 shows data from eight polar ice cores drilled at the Greenland and Antarctic ice sheets that contain a sudden increase in grain size and change in CPO in the lower part of the ice core. The in-situ temperature at the bottom of the boreholes varies significantly between the ice cores. The ice near the bedrock at GISP2 and GRIP was frozen to the bed, while for Byrd, EDC, EDML, NEEM and Siple dome the ice was at, or very close to, pressure-melting point. In all eight ice cores, the CPO and grain size start to change at an in-situ temperature of about -13°C (260K). For the NEEM ice core, this transition coincides with the climatic transition of the end of the Eemian period, also known as marine isotope stage (MIS) 5e, to the beginning of last glacial period (MIS 5d). The transitions to coarse grains with a multi maxima CPO in the EDML, GISP2 and GRIP ice core also coincides with a climatic transition. For the other four ice cores, the transition to a different microstructure does not coincide with a major climatic transition. The pressure corrected temperature threshold (T*, Equation 4-6) at which this transition occurs in these polar ice cores is remarkably constant at T* of -11°C (262K). The depth in the ice cores at which the microstructure changes to large grains and a multi maxima CPO is different for each ice core, which leads to a slightly different T* when correcting for the change in pressure-melting point with depth (Equation 4-6). However, when taking into account the uncertainty in determining the in-situ temperature at a certain depth and the possible influence of the different impurity content between the ice cores and individual layers in the same ice core that affect the pressure-melting point, the effect of correcting the temperature at which the microstructure changes due to changes in overburden pressure is small.

The flow law parameters of the composite flow law (Goldsby and Kohlstedt, 2001) were modified to fit the temperature (T*) threshold of -11°C (262K) for premelting as derived from Table 1 and the experimental data points from Goldsby and Kohlstedt (2001). Another reason for modifying the dislocation creep parameters is improve the fit of the dislocation creep flow law and the experimental data of Goldsby and Kohlstedt (2001) as explained in the companion paper (part 1). Both the flow law parameters for dislocation creep and GBS-limited creep were modified and are given in Table 2. Since the flow law parameters for GBS-limited creep were adjusted to be consistent with a temperature (T*) threshold of 262K, they are different from the flow law parameters used in the companion paper.

Figure 3 shows the temperature versus the calculated strain rate using the original flow law parameters of Glen's flow law (Paterson, 1994) and the end members of the modified flow law parameters of the composite flow law (Table 2). The calculated strain rates for Glen's flow law, dislocation creep and GBS-limited creep increase with increasing temperature and show a kink at their temperature threshold of 263K (Glen's flow law) or 262K (modified composite flow law). The strain rate increase with temperature of the GBS-limited creep mechanism above the temperature threshold of 262K is considerably higher than for the dislocation creep mechanism or Glen's flow law.

The Cryosphere Discuss., https://doi.org/10.5194/tc-2018-275
Manuscript under review for journal The Cryosphere
Discussion started: 20 February 2019

3.4 Calculated strain rates and deformation mechanisms

Figure 4 shows the calculated strain rates, along with the relevant microstructural data (Binder et al., 2013; Eichler et al., 2013; NEEM community members, 2013; Binder, 2014). The modified composite flow law shows that the calculated strain rate in the lower part of the glacial ice, which reaches till a depth of 2207 m (NEEM community members, 2013), is about 2.5 10^{-11} s^{-1} and the CPO has a strong single maximum. The dominant deformation mechanism of the modified composite flow law in the lower part of the glacial ice is GBS-limited creep, with only a very small contribution of dislocation creep to bulk strain rate. Glen's flow law predicts a higher strain rate (about 10^{-10} s^{-1}) than the modified composite flow law in the lower part of the glacial ice. At the interface between the glacial ice and Eemian-glacial facies, the calculated strain rate for the composite flow law drops by about an order of magnitude. The relative contribution of the two end members of the composite flow law changes as well with GBS-limited creep and dislocation creep contributing roughly equally to bulk strain rate. At the same depth, the CPO changes from a strong single maximum in the glacial ice to a partial girdle in the upper part of the Eemian-glacial facies. The calculated strain rate of the modified composite flow law varies by about an order of magnitude between the finer and coarser grained regions close to the stratigraphic disruptions. This variation in calculated strain rate close to the stratigraphic disruptions is produced by GBS-limited creep, which is affected by the change in grain size. The strain rate produced by dislocation creep, which is not affected by the variation in grain size, steadily increases with depth throughout the Eemian-glacial facies. Glen's flow law, which is not affected by grain size variation either, predicts an increasing strain rate with depth and a higher strain rate than the modified composite flow law in the entire Eemian-glacial facies.

The relative contribution of GBS-limited creep and dislocation creep to the bulk strain rate of the modified composite flow law is roughly equal for the ice core sections that were assigned a mean grain diameter of 30 mm just below the stratigraphic disruptions at 2209.6 m and 2262.2 m of depth. At deeper levels, the contribution of GBS-limited creep to bulk strain rate for these coarse grained ice core sections increases. The increase in relative contribution of GBS-limited creep to bulk strain rate, at the assigned constant grain size of 30 mm, results from the lower activation energy at T>262K for dislocation creep compared to GBS-limited creep (Table 2, Figure 3). The difference in activation energy for Glen's flow law and the dislocation creep mechanism above their temperature thresholds is rather small (Table 2), which results in an almost similar strain rate increase with depth.

4 Discussion

The results show that the Eemian-glacial facies consists of layers with relatively fine grains that are alternated by layers of very coarse grains. The coarse grained layers have a strongly interlocking grain boundary structure with a partial girdle type of CPO, while the fine grained layers have a more regular grain shape and have a single maximum type of CPO (Figure 1 and 2). A comparison with other polar ice cores showed that layers with very coarse and interlocking grains with a multi maxima or partial girdle type of CPO start to appear at a T* value of about 262K (Table 1). The modified composite flow

law of Goldsby and Kohlstedt (2001) predicts that the strain rate in the fine grained layers, which is almost entirely produced by GBS-limited creep, is about an order of magnitude higher than the strain rate in the coarse grained layers, where GBS-limited creep and dislocation creep contribute roughly equally to bulk strain rate (Figure 4).

4.1 The role of impurities in premelted ice

It is well known that changes in impurity content correlate well with changes in mean grain size in polar ice cores (e.g. Fisher and Koerner, 1986; Paterson, 1991; Thorsteinsson et al., 1995; Cuffey et al., 2000); finer grains occur in ice with a higher impurity content. It is often assumed that impurities control grain size by pinning of grain boundaries (e.g. Fisher and Koerner, 1986; Gow et al., 1997; Durand et al., 2006), although the exact mechanism by which impurities control the mean grain size is still not understood in detail (Eichler et al., 2017). Similar to the Eemian-glacial facies in the NEEM ice core, the lower part of the GRIP ice core (Thorsteinsson et al., 1995) is likely affected by premelting (Table 1). In both the GRIP and NEEM ice core, the effect of impurities on grain size and shape is very large in the premelting regime (Thorsteinsson et al., 1995; NEEM community members, 2013). Due to the high impurity content in the glacial ice of the Eemian-glacial facies, the mean grain size in these layers remains relatively small. One the other hand, the Eemian ice in the Eemian-glacial facies is not (or hardly) affected by the impurity content and the grains are much larger. The second effect of the high impurity content in the glacial layers in the Eemian-glacial facies is the melt content along grain boundaries and triple junctions is probably enhanced due to the lowering of the pressure-melting point by salts and/or impurities (e.g. Duval, 1977; Wettlaufer, 1999a, b; Döppenschmidt and Budd, 2000).

Impurities also provide additional interfaces, in addition to grain boundaries, where premelting can take place. These premelting films could act as dislocation sinks that may enhance dislocation motion in ice, preventing hardening by dislocation entanglement and thus enhance the strain rate. The type of impurity can change the effectivity of premelting, but as only few studies on particle species in solid polar ice are available so far (Ohno et al., 2005, 2006; Sakurai et al., 2009; 2011; Oyabu et al., 2015), this argument can only be made via the total surface of impurities per volume of ice.

4.2 The effect of premelting on ice microstructure

Premelting is expected to initiate at grain boundaries at temperatures below, but close to, the melting point (e.g. Orem and Adamson, 1969; Döppenschmidt et al., 1998). Since premelting itself, as well as the collection of water in veins (Nye and Mae, 1972), takes place at grain boundaries and triple junctions, grain boundaries are the major ‘suspect’ that enables weakening in polycrystalline ice. As temperature increases, a water-like amorphous layer gathers in layers along grain boundaries and veins along triple junctions, the presence of a water-like amorphous layer correlates with strain rates that are faster than predicted by extrapolation of low temperature results using the Arrhenius relation with a fixed activation energy (e.g. Mellor and Testa, 1969; Nye and Mae, 1972; Duval et al., 1977; Dash et al., 1995; De la Chapelle et al., 1999). Therefore, a flow law that is calibrated at lower temperature cannot simply be applied under premelting conditions, since the mechanical properties of the material at premelting temperature, apparently, are different. Due to the higher grain boundary

surface area per unit of volume in a fine grained sample, the influence of premelting on a fine grained sample is expected to be stronger than for a coarser grained sample.

A small liquid-like amorphous layer at the grain boundaries increases grain boundary mobility by about two to four orders of magnitude (Duval and Castelnau, 1995; Schulson and Duval, 2009). Since grain boundary velocity is a function of grain boundary mobility and the driving force for grain boundary migration (e.g. Higgins, 1974; Alley et al., 1986), it is expected that a strong increase in grain boundary mobility leads to an increase in grain boundary velocity, provided that the stored strain energy for SIBM in the ice polycrystal is high enough. Ice deformation tests have indeed shown that grain boundary migration rates are high close to the melting point (e.g. Wilson and Zhang, 1996; Breton et al., 2016). Microstructural changes ocurring in ice close to the melting point that creates very coarse and interlocking grains, and a change in deformation behaviour, could both well be explained by the presence of a liquid-like amorphous layer that increases grain boundary mobility and consequently enhances SIBM. This enhanced SIBM would result in very coarse grains with an interlocking grain boundary structure (e.g. Duval and Castelnau, 1995; Schulson and Duval, 2009; Breton et al., 2016), as observed in the interglacial layers of the Eemian-glacial facies (Figure 1b).

In addition to the effect of high temperature on grain boundary mobility, the cryostatic pressure in the lower part of polar ice cores (20-23 MPa for NEEM, Equation 5) will further enhance grain boundary mobility (Breton et al., 2016). Directed growth of migrating grain boundaries along subgrain boundaries in specimens deformed at a cryostatic pressure of 20 MPa can lead to a smaller median grain size and a more interlocking microstructure. The smaller grain size of samples deformed at a high cryostatic pressure of 20 MPa compared to samples deformed at atmospheric pressure could be caused by grain dissection (Breton et al., 2016; Steinbach et al., 2017), since this process also depends on SIBM.

The similarity between microstructures with coarse interlocking grains in the lower part of polar ice cores (Table 1, Figure 1b) and the ice microstructure developing during deformation tests close to the melting point suggests that these microstructures are governed by the same processes. It is therefore proposed that the sudden appearance of the coarse grains with an interlocking grain boundary structure in the lower part of polar ice cores is the result of premelting along the grain boundaries, which increases grain boundary mobility and consequently enhances SIBM.

4.3 Setting the temperature threshold for premelting

The in-situ temperature at which coarse and interlocking grains start to appear in polar ice sheets occurs at T^* of about -11°C (262K) (Table 1), falls within the temperature range (258K to 263K) of the transition to a more temperature sensitive deformation mechanism during deformation tests (Mellor and Testa, 1969; Barnes et al., 1971; Weertman, 1983; Paterson, 1994; Goldsby and kohlstedt, 2001). The premelting temperature threshold for Glen's flow law (263K; Paterson, 1994) is 5K and 8K higher than the temperature thresholds for the dislocation creep (258K) mechanism and the GBS-limited creep mechanism (255K) applied by Goldsby and Kohlstedt (2001), respectively. Since the strain rate increase close to the melting point for dislocation creep and GBS-limited creep has been related to premelting along the grain boundaries (Goldsby and Kohlstedt, 2001), a similar temperature threshold can be expected for both deformation mechanisms.

The temperature threshold of 258K proposed by Goldsby and Kohlstedt (2001) for dislocation creep was taken from Kirby et al. (1987), who conducted ice deformation tests at a high confining pressure of 50 MPa. A confining pressure of 50 MPa lowers the pressure-melting point by 3.7K, using the pressure-melting constant for clean ice of $7.4\,10^{-8}\,\mathrm{K\,Pa^{-1}}$ (Hobbs, 1974; Weertman, 1983; Equation 4). This change in pressure-melting point due to the high confining pressure seems not to be considered by Kirby et al. (1987) and Goldsby and Kohlstedt (2001). Therefore, it is argued that the temperature threshold should have been 261.7K instead of 258K. This temperature threshold is much closer to 263K used in Glen's flow law (Paterson, 1994) and practically equal to 262K that was found by analysing ice microstructures of polar ice cores (Table 1). 261.7K is also closer to the temperature threshold proposed by Barnes et al. (1971), who found that the activation energy of ice is much higher between 271K and 265K (120 kJ mol^{-1}) than between 265K and 259K (78.1 kJ mol^{-1}). Similarly, 261.7K is also closer to Mellor and Testa (1969) who found that above 263K the strain rate becomes progressively more temperature dependent when approaching the melting point.

4.4 Recrystallization and deformation mechanisms in the Eemian-glacial facies

The strain rate calculations using the composite flow law (Figure 4) show that the fine grained layers in the Eemian-glacial facies deform predominantly by GBS-limited creep. It is known that the basal slip system is not significantly affected by the cryostatic pressures that are reached in polar ice sheets (e.g. Rigsby, 1958; Cole, 1996). Therefore, basal slip is the main strain producing mechanism in both the coarse and the fine grained layers, but the way basal slip is accommodated (i.e. rate-controlled) is different. Since basal slip provides only two of five independent slip systems required for homogeneous deformation, at least one additional slip system or some other mechanism is required (e.g. Von Mises, 1928; Hutchinson, 1977). Grain boundary sliding is favoured as the accommodating mechanism for basal slip in the Eemian-glacial facies, since the grain boundary area in the impurity-rich and fine grained layers is relatively high and a higher grain boundary area enhances the effect of premelting on deformation behaviour (Barnes et al., 1971). However, compared to the glacial ice between 1419 m to 2207 m of depth (Figure 1b), the grain boundary network in the fine grained layers in the Eemian-glacial facies is relatively irregular with many bulges (Figure 1a). The irregular grain boundary structure is likely a result of enhanced SIBM caused by premelting (Section 4.2). Still, the effect of impurities in these impurity-rich layers is strong enough to prevent the grains from growing into tens of millimetres, like the example of the coarse grained ice core section in Figure 1b, so grain boundary sliding remains an important accommodating mechanism. Due to the limited SIBM in these impurity-rich layers, the grains are longer-lived and can rotate towards a single maximum CPO (e.g. Van der Veen and Whillans, 1994). For these layers, the CPO is a reflection of cumulative strain, just like the CPO in the shallower parts of the ice sheet (e.g. Azuma and Higashi, 1985; Alley, 1988; Budd and Jacka, 1989; Llorens et al., 2016a, b, 2017).

For the coarse grained layers in the Eemian-glacial facies the calculations using the available creep laws predicts that the deformation is not dominated by dislocation creep only, but that it has a substantial GBS-limited creep component going up to 75% at xxx m depth (Figure 4). This would suggest that even in these coarse grained layers the creep behaviour is strongly grain size dependent. The question is whether this grain size dependence is in agreement with the interlocking

grain boundary structure observed in the material (Figure 1b), since such a structure seems inconsistent with assumed sliding along grain boundaries. However, SIBM is highly active in these coarse grained layers and SIBM has been suggested to be a possible accommodating mechanism for basal slip (Pimienta and Duval, 1987; De la Chapelle et al., 1999 ; Duval et al., 2000; Montagnat and Duval., 2000). If so, the flow law for GBS-limited creep is not applicable to these coarse grained materials. Alternatively, the original microstructure might have been obliterated by SIBM. In that case, GBS might have locally accommodated basal slip (Raj and Ashby, 1971), hence basal slip might be accommodated by SIBM coupled by GBS (Drury et al., 1989), and the grain size dependent flow law ($\dot{\varepsilon}_{GBS}$) might still be of relevance.

The grain size and grain shape in these impurity-depleted interglacial layers (Figure 1b) suggests that the grain boundaries are free to migrate at the high SIBM rates caused by premelting (Duval and Castelnau, 1995; Schulson and Duval, 2009) and are not or hardly influenced by impurities. The CPO of these coarse grained ice core sections suggests that new grains with a high Schmidt factor nucleate continuously (e.g. Alley, 1988; Montagnat et al., 2015; Qi et al., 2017). A high Schmidt factor indicates grains with a high resolved shear stress on the basal plane, i.e. grains with a soft orientation. Normalized grain size distributions and CPO data from the premelting layer (ice at 262K<T*<273K) in the EDC ice core (Durand et al., 2009) showed that small grains were much more abundant in layers with a multi maxima CPO compared to layers with a single maximum CPO. This strongly suggests that the multi maxima CPO in the premelting layer is linked to the formation of new strain free grains with soft orientations (high Schmidt factor), which grow at the expense of grains oriented in a hard orientation. This recrystallization mechanism can be described as discontinuous migration recrystallization (Wenk et al., 1989; Schulson and Duval, 2009) or SIBM-N (Faria et al., 2014).

4.5 Strain localization in the Eemian-glacial facies

The ice in the Eemian-glacial facies alternates between fine grained ice with a single maximum CPO and coarse grained ice with a partial girdle CPO (Figure 4). The differences in grain size, grain shape and CPO in the Eemian-glacial facies indicates that there are large differences in viscosity between the different layers. This is also shown by the results using the modified composite flow law (Figure 4), that suggest that the fine grained ice is much softer than the coarse grained ice. Consequently, strain localization and strain partitioning into ‘hard’ and ‘soft’ layers can be expected. Strain localization has been shown on many different scales in ice (e.g. Paterson, 1991; Wilson and Zhang, 1996; Grennerat et al., 2012; Jansen et al., 2016; Steinbach et al., 2016). In addition to a variation in grain size, the CPO has also been shown to influence strain rates (e.g. Alley, 1988; Hudleston, 2015). Deformation experiments with ice from other polar ice cores with a certain type of CPO, such as a single maximum or a multi maxima CPO, have different strain rates when the ice is deformed under different deformation modes. For example, simple shear deformation experiments on basal ice with a multi maxima CPO from Law Dome showed that the strain rates were comparable with those of isotropic ice (Russell-Head and Budd, 1979). The same study showed that samples from Law Dome with a single maximum CPO deformed much more readily than isotropic ice in simple shear (sheared in the direction of the measured surface velocity). The study of Lile (1978) with samples from Law Dome and Dome Summit showed a similar result with samples containing a single maximum CPO that were deformed in

simple shear (single maximum normal to the shear plane) showing much higher strain rates compared to laboratory-prepared isotropic ice with a silimar grain size. Samples with a multi maxima CPO from Dome Summit showed a similar strain rate as laboratory-prepared isotropic samples during uniaxial compression tests (Lile, 1978).

On the basis of the variation in grain size and CPO taking into account the literature on deformation modes in ice (above) as well as our results of applying the modified composite flow law (Figure 4), it is hypothesized that deformation of ice in the Eemian-glacial facies is partitioned in simple shear mode with fast deformation in the fine grained layers with a single maximum CPO (e.g. Figure 1a), and coaxial mode with slower deformation in the coarse grained layers with a partial girdle CPO (e.g. Figure 1b). Simple shear is indeed expected to be the dominant deformation mode in this part of the NEEM ice core (Dansgaard and Johnsen, 1969; Montagnat et al., 2014). The likely partitioning of deformation into simple shear in the fine grained layers with a single maximum CPO results in a positive feedback loop as deformation by simple shear enhances the strength of the single maximum CPO making the ice even softer.

The composite flow law that is used in this study does not explicitely include the effect of CPO on strain rate, while it is well known that the CPO has a weakening effect on ice depending on its orientation in certain different deformation modes (e.g. Alley, 1988; Hudleston, 2015). Therefore, the partitioning of strain into layers with different CPO's can produce additional variations in strain rate on top of the strain rate variations presented in Figure 4. The fine grained layers have a CPO that is compatible with the main deformation mode in this part of the NEEM ice core (simple shear), while the coarse grained layers do not have a compatible CPO and are likely relatively stagnant or deform in coaxial deformation. Therefore, it is likely that the difference in strain rate between the fine grained and coarse grained layers in the Eemian-glacial facies is even larger than shown in Figure 4. The relatively fine grained layer (5-10 mm) with a partial girdle CPO between 2265 m and 2365 m of depth (example in Figure 1c) represents a 'mixed case' between the two end members consisting of (i) layers with fine grain size with a single maximum CPO and (ii) layers with coarse and interlocking grains with a partial girdle CPO. Since the CPO of this layer (Figure 1c) is relatively hard in simple shear, which is the dominant deformation mode at this depth, it is likely that the layer between 2265 m and 2365 m of depth deforms at a lower strain rate than predicted in Figure 4.

The difference in microstructure between the impurity-rich glacial ice and the impurity-depleted interglacial ice poses an interesting hypothesis for the effect of premelting on ice dynamics close to the bedrock. In the case where the premelting layer consists entirely of interglacial ice (with a low impurity content) the premelting layer is expected to be relatively stagnant, provided the bedrock topography allows this, and hardly contributes to horizontal velocity, which will probably be localized above the premelting layer. In the case where glacial ice (with a high impurity content) is present in the premelting layer or the premelting layer consists entirely of glacial ice, a significant portion of the horizontal velocity will be accomplished in the premelting layer. The difference in microstructure of impurity-rich glacial and impurity-depleted interglacial ice in the premelting layer can have important consequences for ice dynamics close to the bedrock. Since the impurity content in the Greenland ice sheet is approximately 10 times higher than the impurity content in the Antarctic ice

sheet (e.g. Legrand and Mayewski, 1997), this effect of strain partitioning in the premelting layer is likely to be stronger in the Greenland ice sheet than in the Antarctic ice sheet.

Borehole data from Byrd station showed that the tilting rate (deformation rate) in the premelting layer (1810 m down to the bedrock at 2164 m of depth), where grains are coarse with a multi maxima CPO (Gow and Williamson, 1976), deformed much less than the remainder of the ice (Paterson, 1983). Borehole data from the deeper part of the EDML ice core showed that a coarse grained layer with a girdle type CPO deformed predominantly by pure shear, while the layers just above and below deformed predominantly by simple shear (Jansen et al., 2017). Both these layers show a similar microstructure compared to the Eemian-glacial facies: the layer that deforms by coaxial deformation consists of coarse grains with a multi-maxima or partial girdle type of CPO, while the layers above and below deform by simple shear and consist of finer grains with a single maximum CPO. Borehole data from the lower part of the NEEM ice core might confirm whether the strain rate variability with depth in the premelting layer is as large as predicted in Figure 4.

Strain partitioning between glacial and interglacial layers in the premelting zone can lead to a different rate of layer thinning. Coaxial deformation clearly leads to layer thinning, while deformation by simple shear alone, does not lead to layer thinning if the shear plane is parallel to the layering. Therefore, the layers in the coarse grained regions with a multi maxima or partial girdle type CPO could be thinning at a higher rate than the fine grained regions with a single maximum CPO. Even if in reality we can assume general shear (mixed simple shear and coaxial deformation), the relative importance or impact of a likely unequal share of both deformation modes will lead to differing thinning rates.

The heterogeneous deformation between the layers, and particularly heterogeneous layer thinning, can have important consequences for interpreting paleoclimatic records from polar ice cores, as in the deepest part of the ice core the dating tool is based on ice flow modelling describing a homogeneus transition from coaxial deformation to simple shear. It has often been shown that paleoclimatic records in the lower part of polar ice cores are disturbed (e.g. Alley et al., 1997; Gow et al., 1997; Suwa et al., 2006; Ruth et al.; 2007; NEEM community members, 2013), which could be caused by heterogeneous deformation and strain partitioning between glacial and interglacial layers as described above. The suggestion of hetrogeneous layer thinning as proposed above is still speculative and further research on this topic is needed.

5 Conclusions

In many polar ice cores the grain size, grain shape and CPO change significantly in the ice close to the bedrock, which can have a large impact on the dominant deformation mechanism and the strain rate. In this study, actual temperature and grain size data of the NEEM ice core were used to apply the composite flow law of Goldsby and Kohlstedt (2001) and Glen's flow law (1955) to the lower part of the NEEM ice core with the aim of studying the effect of changes in grain size on the dominant deformation mechanism and the strain rate. Several stratigraphic disruptions are present in this part of the NEEM ice core, which causes layers of fine grained glacial ice to be alternated by layers of coarse grained Eemian ice. After a microstructural evaluation of eight different polar ice cores from the Greenland and Antarctic ice sheets, it was found that

microstructures that indicate premelting start at a temperature (T*) of about 262K, which is within the temperature range at which a more temperature sensitive deformation mechanism starts to dominate the ice rheology in deformation tests. The composite flow law of Goldsby and Kohlstedt (2001) was modified to include this premelting temperature (T*) threshold of 262K.

The modified composite flow law predicts that, as a result of the grain size variation in the Eemian-glacial facies, the strain rate varies strongly with the fine grained layers deforming about an order of magnitude faster than the coarse grained layers. In the fine grained glacial ice the dominant deformation mechanism is predicted to be GBS-limited creep. In the coarse grained interglacial ice, dislocation creep and GBS-limited creep contribute roughly equally to the bulk strain rate, with the contribution of GBS-limited creep to bulk strain rate increasing with depth. Glen's flow law, which is grain size insensitive, is unable to predict the strong variations in strain rate in the Eemian-glacial facies and predicts a steadily increasing strain rate with depth caused by an increase in temperature with depth. Glen's flow law predicts a higher strain rate than the modified composite flow law along the entire lowest 540 m of depth of the NEEM ice core.

Changes in grain size in the Eemian-glacial facies correlate strongly with changes in type and strength of CPO. The fine grained (<5 mm) impurity-rich glacial layers have a strong single maximum CPO, which is compatible with predominant simple shear deformation in this part of the NEEM ice core. The relatively fine grain size argues for GBS-limited creep to be the dominant deformation mechanism in these layers. The coarse grained (>5 mm) impurity-depleted interglacial layers have a partial girdle type of CPO, which is more compatible with coaxial deformation than with simple shear deformation. Due to the coarse grains and the interlocking grain boundary structure, these layers are likely deforming by basal slip accommodated by recovery via SIBM, which removes dislocations and stress concentrations in grains and allows further deformation to occur, or by coupled SIBM and grain boundary sliding. Therefore, strain partitioning is expected in the Eemian-glacial facies with the fine grained glacial layers with a single maximum CPO deforming at high strain rates in simple shear, while the coarse grained interglacial layers with a partial girdle type of CPO deform at much lower strain rates by coaxial deformation. The difference in microstructure, and consequently difference in viscosity, of impurity-rich glacial and impurity-depleted interglacial ice in the premelting layer can have important consequences for ice dynamics close to the bedrock.

Acknowledgements

This work has been carried out as part of the Helmholtz Junior Research group "The effect of deformation mechanisms for ice sheet dynamics" (VH-NG-802). The NEEM light microscope data used in this study has been made available by www.pangaea.de. The authors would like to thank Sepp Kipfstuhl and Tobias Binder for providing data and encouraging discussions. The authors would like to thank all the NEEM Community members who were involved in the preparation of the physical properties samples in the field. This work is a contribution to the NEEM ice core project which is directed and organized by the Center of Ice and Climate at the Niels Bohr Institute and US NSF, Office of Polar Programs. It is supported

by funding agencies and institutions in Belgium (FNRS-CFB and FWO), Canada (NRCan/GSC), China (CAS), Denmark (FIST), France (IPEV, CNRS/INSU, CEA and ANR), Germany (AWI), Iceland (RannIs), Japan (NIPR), South Korea (KOPRI), the Netherlands (NWO/ALW), Sweden (VR), Switzerland (SNF), the Unites Kingdom (NERC) and the USA (US NSF, Office of Polar Programs).

References

Alley, R. B.: Fabrics in Polar Ice Sheets: Development and Predictions. Science, 240, 493-495, doi:10.1126/science.240.4851.493, 1988.

Alley, R. B.: Flow-law hypothesis for ice sheet modeling. Journal of Glaciology, 38, 245-256, doi:10.1017/S0022143000003658, 1992.

Alley, R. B., Gow, A. J., Meese, D. A., Fitzpatrick, J. J., Waddington, E. D., and Bolzan, J. F.: Grain-scale processes, folding, and stratigraphic disturbance in the GISP2 ice core. Journal of Geophysical Research, 102, 26819-26830, doi:10.1029/96JC03836, 1997.

Alley, R. B., Perepezko, J. H., and Bentley, C. R.: Grain growth in polar ice: I. Theory. Journal of Glaciology, 32, 415-424, 1986.

Augustin, L., Panichi, S., and Frascati, F.: EPICA Dome C 2 drilling operations: performances, difficulties, results. Annals of Glaciology, 47, 68-72, doi:10.3189/172756407786857767, 2007.

Azuma, N., and Higashi, A.: Formation processes of ice fabric pattern in ice sheets. Annals of Glaciology, 6, 130-134, 1985.

Barnes, P., Tabor, D., and Walker, J. C. F.: The friction and creep of polycrystalline ice. Proceedings of the Royal Society London A., 324, 127-155, 1971.

Binder, T., Weikusat, I., Freitag, J., Garbe, C. S., Wagenbach, D., and Kipfstuhl, S.: Microstructure through an ice sheet. Materials Science Forum, 753, 481-484, doi:10.4028/www.scientific.net/MSF.753.481, 2013.

Binder, T.: Measurements of grain boundary networks in deep polar ice cores – A digital image processing approach. PhD thesis, University of Heidelberg, Germany, 2014.

Breton, D. J., Baker, I., and Cole, D. M.: Microstructural evolution of polycrystalline ice during confined creep testing. Cold Regions Science and Technology, 127, 25-36, doi:10.1016/j.coldregions.2016.03.009, 2016.

Budd, W. F., and Jacka, T. H.: A review of ice rheology for ice sheet modelling. Cold Regions Science and Technology, 16, 107-144, doi:10.1016/0165-232X(89)90014-1, 1989.

Budd, W. F., and Rowden-Rich, R. J. M.: Finite element analysis of two-dimensional longitudinal section flow on Law Dome. Australian Glaciological Research; 1982-1983. ANARE Res. Notes, 28: 153-161, 1985.

Buizert, C., Cuffey, K. M., Severinghaus, J. P., Baggenstos, D., Fudge, T. J., Steig, E. J., Markle, B. B., Winstrup, M., Rhodes, R. H., Book, E. J., Sowers, G. D., Clow, G. D., Cheng, H., Edwards, R. L., Sigl, M., McConnell, J. R., and Taylor,

K. C.: The WAIS Divide deep ice core WD2014 chronology – Part 1: Methane synchronization (68-31 ka BP) and the gas age-ice age difference. Climate of the Past, 11, 153-173, doi:10.5194/cp-11-153-2015, 2015.

Catania, G. A., and Neumann, T. A.: Persistent englacial drainage features in the Greenland Ice Sheet. Geophysical Research Letters, 37, 1-5, doi: 10.1029/2009GL041108, 2010.

Cole, D. M.: Observations of pressure effects on the creep of ice single crystals. Journal of Glaciology, 42, 169-175, doi:10.1017/S0022143000030628, 1996.

Cuffey, K. M., Thorsteinsson, T., and Waddington, E. D.: A renewed argument for crystal size control of ice sheet strain rates. Journal of Geophysical Research, 105, 27889-27894, doi:10.1029/2000JB900270, 2000.

Dash, J. G., Fu, H., and Wettlaufer, J. S.: The premelting of ice and its environmental consequences. Reports on Progress in Physics, 58, 115-167, doi:10.1088/0034-4885/58/1/003, 1995.

Dash, J. G., Rempel, A. W., and Wettlaufer, J. S.: The physics of premelted ice and its geophysical consequences. Reviews of Modern Physics, 78, 695-741, doi:10.1103/RevModPhys.78.695, 2006.

Dansgaard, W., Johnsen, S. J.: A flow model and a time scale for the ice core from camp century, Greenland. Journal of Glaciology, 8, 215-223, doi:10.3189/S0022143000031208, 1969.

De La Chapelle, S., Milsch, H., Castelnau, O., and Duval, P.: Compressive creep of ice containing a liquid intergranular phase: rate-controlling processes in the dislocation creep regime. Geophysical Research Letters, 26, 251-254, doi:10.1029/1998GL900289, 1999.

Doake, C. S. M., and Wolff, E. W.: Flow law for ice in polar ice sheets. Nature, 314, 6008, 255-257, doi:10.1038/314255a0, 1985.

Döppenschmidt, A., and Butt, H.-J.: Measuring the Thickness of the Liquid-like Layer on Ice Surfaces with Atomic Force Microscopy, Langmuir, 16, 6709-6714, doi:10.1021/la990799w, 2000.

Döppenschmidt, A., Kappl, M., and Butt, H. J.: Surface Properties of Ice Studied by Atomic Force Microscopy. Journal of Physical Chemistry, 102, 7813-8919, doi:10.1021/jp981396s, 1998.

Drury, M. R., Humphreys, F. J., and White, S. H.: Effect of dynamic recrystallization on the importance of grain-boundary sliding during creep. Journal of Materials Science, 24, 154-162, doi:10.1007/BF00660947, 1989.

Durand, G., Svensson, A., Persson, A., Gagliardini, O., Gillet-Chaulet, F., Sjolte, J., Montagnat, M., and Dahl-Jensen, D.: Evolution of the texture along the EPICA Dome C ice core. Low Temperature, Science, 68, 91-105, 2009.

Durand, G., Weiss, J., Lipenkov, V., Barnola, J. M., Krinner, G., Parrenin, F., Delmonte, B., Ritz, C., Duval, P., Röthlisberger, R., and Bigler, M.: Effect of impurities on grain growth in cold ice sheets. Journal of Geophysical Research, 111, 1-18, doi:10.1029/2005JF000320, 2006.

Durham, W. B., and Stern, L. A.: Rheological Properties of Water Ice – Applications to satellites of the Outer Planets. Annual Review of Earth and Planetary Science, 29, 295-330, 2001.

Duval, P.: The role of the water content on the creep rate of polycrystalline ice. International Association of hydrological Sciences, 118, 29-33, 1977.

Duval, P., Arnaud, L., Brissaud, O., Montagnat, M., and De La Chapelle, S.: Deformation and recrystallization processes of ice from polar ice sheets. Annals of Glaciology, 30, 83-87, doi:10.3189/172756400781820688, 2000.

Duval, P., and Castelnau, O.: Dynamic Recrystallization of Ice in Polar Ice Sheets. Journal de Physique III, 05, 197-205, doi:10.1051/jp4:1995317, 1995.

Eichler, J., Weikusat, I., and Kipfstuhl, S.: Orientation-tensor eigenvalues along the NEEM ice core. PANGAEA, https://doi.org/10.1594/Pangaea.838059, 2013.

Eichler, J., Kleitz, I., Bayer-Giraldi, M., Jansen, D., Kipfstuhl, S., Shigeyama, W., Weikusat, C., and Weikusat, I.: Location and distribution of micro-inclusions in the EDML and NEEM ice cores using optical microcopy and in situ Raman spectroscopy. The Cryosphere, 11, 1075-1090, doi:10.5194/tc-11-1075-2017, 2017.

Eichler, J., Weikusat, C., Wegner, A., Twarloh, B., Behrens, M., Fischer, H., Hoerhold, M., Jansen, D., Kipfstuhl, S., Ruth, U., Wilhelms, F., and Weikusat, I: Impurity analysis and microstructure along the climatic transition from MIS 6 into 5e in the EDML ice core using cryo-Raman microscopy. Submitted to Frontiers in Earth Science on 07 September 2018, submitted.

EPICA community members: Eight glacial cycles from an Antarctic ice core. Nature, 429, 623-628, doi:10.1038/nature02599, 2004.

Epstein, S., Sharp, R. P., and Gow, A. J.: Antarctic Ice Sheet: Stable Isotope Analysis of Byrd Station Cores and Interhemispheric Climate Implications. Science, 168, 1570-1572, doi:10.1126/science.168.3939.1570, 2011.

Faria, S. H., Weikusat, I., and Azuma, N.: The microstructure of polar ice: Part II: State of the art. Journal of Structural Geology, 61, 21-49, doi:10.1016/j.jsg.2013.11.003, 2014.

Fitzpatrick, J. J., Voigt, D. E., Fegyveresi, J. M., Stevens, N. T., Spencer, M. K., Cole-Dai, J., Alley, R. B., Jardine, G. E., Cravens, E. D., Wilen, L. A., Fudge, T. J., and McConnell, J. R.: Physical properties of the WAIS Divide ice core. Journal of Glaciology, 69, 1181-1198, doi:10.3189/2014JoG14J100, 2014.

Fisher, D. A., and Koerner, R. M.: On the special rheological properties of ancient microparticle-laden northern hemisphere ice as derived from bore-hole and core measurements. Journal of Glaciology, 32, 501-510, 1986.

Glen, J. W.: Experiments on the deformation of ice. Journal of Glaciology, 2, 111-114, 1952.

Glen, J. W.: The creep of polycrystalline ice. Proceedings of the Royal Society London A., 228, 519-538, doi:10.1098/rspa.1955.0066, 1955.

Goldsby, D. L., and Kohlstedt, D. L.: Grain boundary sliding in fine grained ice I. Scripta Materialia, 37, 1399-1406, 1997.

Goldsby, D. L., and Kohlstedt, D. L.: Superplastic deformation of ice: Experimental observations. Journal of Geophysical Research, 106, 11017-11030, doi:10.1029/2000JB900336, 2001.

Goldsby D. L.: Glacier Science and environmental change (eds. by P. G. Knight). pp. 308-314. Blackwell, Oxford, 2006.

Gow, A. J., and Engelhardt, H.: Preliminary analysis of ice cores from Siple Dome, West Antarctica. In Hondoh, T., ed. Physics of ice core records. Sapporo, Hokkaido University Press, 63–82, 2000.

Gow, A. J., Meese, D. A., Alley, R. B., Fitzpatrick, J. J., Anandakrishnan, S., Woods, G. A., and Elder, B. C.: Physical and structural properties of the Greenland Ice Sheet Project 2 ice core: A review. Journal of Geophysical Research, 102, 26559-26575, doi:10.1029/97JC00165, 1997.

Gow, A. J., and Williamson, T.: Rheological implications of the internal structure and crystal fabrics of the West Antarctic ice sheet as revealed by deep core drilling at Byrd Station. Bulletin of the Geological Society of America, 87, 1665-1677, 1976.

Grennerat, F., Montagnat, M., Castelnau, O., Vacher, P., Moulinec, H., Suquet, P., and Duval, P.: Experimental characterization of the intragranular strain field in columnar ice during transient creep. Acta Materialia, 60, 3655-3666, doi:10.1016/j.actamat.2012.03.025, 2012.

Gudlaugsson, E., Humbert, A., Kleiner, T., Kohler, J., and Andreassen, K.: The influence of a model subglacial lake on ice dynamics and internal layering. Cryosphere, 10, 751-760, doi:10.5194/tc-10-751-2016, 2016.

Hammer, C. U., Clausen, H. B., and Langway, C. C.: Electrical conductivity method (ECM) stratigraphic dating of the Byrd Station ice core, Antarctica. Annals of Glaciology, 20, 155-120, doi:10.3189/172756494794587555, 1994.

Higgins, G. T.: Grain-boundary migration and grain growth. Metal Science, 8, 143-150, doi:10.1179/msc.1974.8.1.143, 1974.

Hobbs, P. V.: Ice Physics, Clarendon Press, Oxford, 1974.

Homer, D. R., and Glen, J. W.: The creep activation energies of ice. Journal of Glaciology, 21, 429-444, doi:10.3189/S0022143000033591, 1978.

Hudleston, P. J.: Structures and fabrics in glacial ice: A review. Journal of Glaciology, 81, 1-27, doi:10.1016/j.jsg.2015.09.003, 2015.

Humphreys, F. J., and Hatherly, M.: Recrystallization and Related Annealing Phenomena. Oxford, Elsevier, 2004.

Hutchinson, J. W.: Creep and Plasticity of Hexagonal Polycrystals as Related to Single Crystal Slip. Metallurgical Transactions A, 8, 1465-1469, doi:10.1007/BF02642860, 1977.

IPCC.: Climate change 2014: Synthesis report. contribution of working groups i, ii, iii to the fifth assessment report of the intergovernmental panel on climate change, IPCC, Geneva, Switzerland, 151, 2014.

Jansen, D., Llorens, M.-G. Westerhoff, J., Steinbach, F., Kipfstuhl, S., Bons, P. D., Griera, A., and Weikusat, I.: Small-scale disturbances in the stratigraphy of the NEEM ice core: observations and numerical model simulations. The Cryosphere, 10, 359-370, doi:10.5194/tc-10-359-2016, 2016.

Jansen, D., Weikusat, I., Kleiner, T., Wilhelms, F., Dahl-Jensen, D., Frenzel, A., Stoll, N., Binder, T., Eichler, J., Faria, S. H., Sheldon, S., Panton, C., Kipfstuhl, S., and Miller, H.: In situ-measurement of ice deformation from repeated borehole logging of the EPICA Dronning Maud Land (EDML) ice core, East Antarctica. Poster presentation, EGU, Vienna (Austria). https://meetingorganizer.copernicus.org/EGU2017/EGU2017-16368.pdf, 2017

Johnsen, S. J., Dahl-Jensen, D., Dansgaard, W., and Gundestrup, N.: Greenland paleotemperatures derived from GRIP bore hole temperature and ice core isotope profiles. Tellus B, 47, 624-629, doi:10.1034/j.1600-0889.47.issue5.9.x, 1995.

Jones, J., and Brunet, J. G.: Deformation of ice single crystals close to the melting point. Journal of Glaciology, 21, 445-455, 1978.

Kipfstuhl, S.: Large area scan macroscope images from the NEEM ice core. Alfred Wegener Institute, Helmholtz Center for Polar and Marine Research, Bremerhaven, Pangaea, https://doi.pangaea.de/10.1594/PANGAEA.743296 (unpublished dataset), 2010.

Kipfstuhl, S., Hamann, I., Lambrecht, A., Freitag, J., Faria, S. H., Grigoriev, D., and Azuma, N.: Microstructure mapping: a new method for imaging deformation induced microstructural features of ice on the grain scale, Journal of Glaciology, 52, 178, 398-406, doi:10.3189/172756506781828647, 2006.

Kipfstuhl, S., Faria, S. H., Azuma, N., Freitag, J., Hamann, I., Kaufmann, P., Miller, H., Weiler, K., and Wilhelms, F.: Evidence of dynamic recrystallization in polar firn. Journal of Geophysical Research: Solid Earth, 114, 1-10, doi:10.1029/2008JB005583, 2009.

Kirby, S., Durham, W., Beeman, M., Heard, H., and Daley, M.: Inelastic properties of ice I_h at low temperatures and high pressures. Journal de Physique Colloques, 48, 227-232, doi:10.1051/jphyscol:1987131, 1987.

Kopp, R. E., DeConto, R. M., Bader, D. A., Hay, C. C., Horton, R. M., Kulp, S., Oppenheimer, M., Pollard, D., and Strauss, B. H.: Evolving understanding of Antarctic ice-sheet physics and ambiguity in probabilistic sea-level projections. Earth's Future, 5, 1-17, doi:10.1002/2017EF000663, 2017.

Krabbendam, M.: Sliding of temperate basal ice on a rough, hard bed: creep mechanisms, pressure melting, and implications for ice streaming. The Cryosphere, 10, 1915-1932, doi:10.5194/tc-10-1915-2016, 2016.

Krischke, A., Oechsner, U., and Kipfstuhl, S.: Rapid Microstructure Analysis of Polar Ice Cores. Optik & Photonik, WILEY-VCH Verlag, Weinheim, 10, 32-35, 2015.

Legrand, M., and Mayewski, P.: Glaciochemistry of polar ice cores: A review. Reviews of Geophysics, 35, 219-243, doi:10.1029/96RG03527, 1997.

Lile, R. C.: The effect of anisotropy on the creep of polycrystalline ice. Journal of Glaciology, 21, 475-483, 1978.

Lisiecki, L. E., and Raymo, M. E.: A Pliocene-Pleistocene stack of 57 globally distributed benthic $\delta^{18}O$ records. Paleoceanography, 20, 1-17, doi:10.1019/2004PA001071, 2005.

Lliboutry, L.: Physical processes in temperate glaciers. Journal of Glaciology, 16, 151-158, doi:10.3189/S002214300003149X, 1976.

Llorens, M.-G., Griera, A., Steinbach, F., Bons, P. D., Gomez-Rivas, E., Jansen, D., Roessiger, J., Lebensohn, R. A., and Weikusat, I.: Dynamic recrystallization during deformation of polycrystalline ice: insights from numerical simulations. Philosophical Transactions A, A375, 2086, doi:10.1098/rsta.2015.0346, 2017.

Llorens, M.-G., Griera, A., Bons, P. D., Roessiger, J., Lebensohn, R., Evans, L., and Weikusat, I.: Dynamic recrystallisation of ice aggregates during co-axial viscoplastic deformation: a numerical approach. Journal of Glaciology, 62, 359-377, doi:10.1017/jog.2016.28, 2016a.

Llorens, M.-G., Griera, A., Bons, P., Lebensohn, R. A., Evans, L. A., Jansen, D., and Weikusat, I.: Full-field predictions of ice dynamic recrystallization under simple shear conditions. Earth and Planetary Science Letters, 450, 233-242, doi:10.1016/j.epsl.2016.06.045, 2016b.

Mellor, M., and Testa, R.: Effect of temperature on the creep of ice. Journal of Glaciology, 8, 131-145, 1969.

Montagnat, M., Chauve, T., Barou, F., Tommasi, A., Beausir, B., and Fressengaes, C.: Analysis of Dynamic Recrystallization of Ice from EBSD Orientation Mapping. Frontiers in Earth Science, 3, 1-13, doi:10.3389/feart.2015.00081, 2015.

Montagnat, M., and Duval, P.: Rate controlling processes in the creep of polar ice, influence of grain boundary migration associated with recrystallization. Earth and Planetary Science Letters, 183, 179-186, doi:10.1016/S0012-821X(00)00262-4, 2000.

Montagnat, M., Azuma, N., Dahl-Jensen, D., Eichler, J., Fujita, S., Gillet-Chaulet, F., Kipfstuhl, S., Samyn, D., Svenson, A., and Weikusat, I.: Fabric along the NEEM ice core, Greenland, and its comparison with GRIP and NGRIP ice core. The Cryosphere, 8, 1129-1138, doi:10.5194/tc-8-1129-2014, 2014.

Morgan, V. I.: High-temperature ice creep tests. Cold Regions Science and Technology, 19, 295-300, doi:10.1016/0165-232X(91)90044-H, 1991.

NEEM community members: Eemian interglacial reconstructed from a Greenland folded ice core. Nature, 493, 489-493, doi:10.1038/nature11789, 2013.

Nereson, N. A., Waddington, E. D., Raymond, C. F., and Jacobson, H. P.: Predicted age-depth scales for Siple Dome and inland WAIS ice cores in West Antarctica. Geophysical Research Letters, 23, 3163-3166, doi:10.1029/96GL03101, 1996.

Nye, J. F., and Mae, S.: The effect of non-hydrostatic stress on intergranular water veins and lenses in ice. Journal of Glaciology, 11, 81-101, doi:10.3189/S0022143000022528, 1972.

Ohno, H., Igarashi, M., and Hondoh, T.: Salt inclusions in polar ice core: Location and chemical form of water-soluble impurities. Earth and Planetary Letters, 232, 171-178, doi:10.1016/j.epsl.2005.01.001, 2005.

Ohno, H., Igarashi, M., and Hondoh, T.: Characteristics of salt inclusions in polar ice from Dome Fuji, East Antarctica, Geophysical Research Letters, 33, 1-5, doi:10.1029/2006Gl025774, 2006.

Orem, M. W., and Adamson, A. W.: Physical adsorption of Vapor on ice. Journal of Colloid and Interface Science, 31, 278-286, doi:10.1016/0021-9797(69)90337-3, 1969.

Oyabu, I., Lizuka, Y., Fisher, H., Schüpbach, S., Gfeller, G., Svensson, A., Fukui, M., Steffensen, J. P., and Hansson, M.: Chemical composition of particles present in the Greenland NEEM ice core over the last 110,000 years. Journal of Geophysical Research: Atmospheres, 120, 9789-9813, doi:10.1002/2015JD023290, 2015.

Paterson, W. S. B.: Deformation within polar ice sheets: an analysis of the Byrd station and Camp Century borehole-tilting measurements. Cold Regions Science and Technology, 8, 165-179, 1983.

Paterson, W. S. B.: Why ice-age ice is sometimes “soft”. Cold Regions Science and Technology, 20, 75-98, doi:10.1016/0165-232X(91)90058-O, 1991.

Paterson, W. S. B.: The physics of glaciers. Third edition. Oxford, Elsevier, 1994.

Pimienta, P., and Duval, P.: Rate controlling processes in the creep of polar glacier ice. Journal de Physique Colloques, 48, 243-248, doi:10.1051/jphyscol:1987134, 1987.

Qi, C., Goldsby, D. L., and Prior, D. J.: The down-stress transition from cluster to cone fabrics in experimentally deformed ice. Earth and Planetary Science Letters, 471, 136-147, doi:10.1016/j.epsl.2017.05.008, 2017.

Raj, R., and Ashby, M. F.: On grain boundary sliding and diffusional creep. Metallurgical Transactions, 2, 1113-1127, doi:10.1007/BF02664244, 1971.

Rasmussen, S. O., Abbott, P. M., Blunier, T., Bourne, E., Brook, E., Buchardt, S. L., Buizert, C., Chappellaz, J., Clausen, H. B., Cook, E., Dahl-Jensen, D., Davies, S. M., Guillevic, M., Kipfstuhl, S., Laepple, T., Seierstad, I. K., Severinghaus, J. P., Steffensen, J. P., Stowasser, C., Svensson, A., Vallelonga, P., Vinther, B. M., Wilhelms, F., and Winstrup, M.: A first chronology for the North Greenland Eemian Ice Drilling (NEEM) ice core. Climate of the past, 9, 2713-2730, doi:10.5194/cp-9-2713-2013, 2013.

Rigsby, G. P.: Effect of hydrostatic pressure on velocity of shear deformation of single ice crystals. Journal of Glaciology, 3, 273-278, doi:10.3189/S0022143000023911, 1958.

Rogozhina, I., Petrunin, A. G., Vaughan, A. P. M., Steinberger, B., Johnson, J., Kaban, M. K., Calov, R., Rickers, F., Thomas, and M., Koulakov, I.: Melting at the base of the Greenland ice sheet explained by Iceland hotspot history. Nature Geosciences, 9, 366-369, doi:10.1038/NGEO2689, 2016.

Russell-head, D. S., and Budd, W. F.: Ice-sheet flow properties derived from bore-hole shear measurements combined with ice-core studies. Journal of Glaciology, 24, 117-130, doi:10.3189/S0022143000014684, 1979.

Ruth, U., Barnola, J.-M., Beer, J., Bigler, M., Castellano, E., Fisher, H., Fundel, F., Huybrechts, P., Kaufmann, P., Kipfstuhl, S., Lambrecht, A., Morganti, A., Oerter, H., Parrenin, F., Rybak, O., Severi, M., Udisti, R., Wilhelms, F., and Wolff, E.: "EDML 1": a chronology of the EPICA deep ice core from Dronning Maud Land, Antarctica, over the last 150 000 years. Climate of the Past, 3, 475-484, doi:10.5194/cp-3-475-2007, 2007.

Sakurai, T., Iizuka, Y., Horlkawa, S., Johnsen, S., Dahl-Jensen, D., Steffensen, J. P., and Hondoh, T.: Direct observations of salts as micro-inclusions in the Greenland GRIP ice core. Journal of Glaciology, 55, 777-783, doi:10.3189/002214309790152483, 2009.

Sakurai, T., Ohno, H., Horikawa, S., Iizuka, Y., Uchida, T., Hirakawa, K., and Hondoh, T.: The chemical forms of water-soluble microparticles preserved in the Antarctic ice sheet during Termination I. Journal of Glaciology, 57, 1027-1032, doi:10.3189/002214311798843403, 2011.

Saylor, M. S., and Rohrer, G. S.: Measuring the Influence of Grain-Boundary Misorientation on Thermal Groove Geometry in Ceramic Polycrystals. Journal of the American Society, 82, 1529-1536, doi:10.1111/j.1151-2916.1999.tb01951.x, 1999.

Schulson, E. M., and Duval, P.: Creep and Fracture of Ice. Cambridge University Press, Cambridge, 2009.

Sheldon, S. G., Steffensen, J. P., Hansen, S. B., Popp, T. J., and Johnsen, S. J.: The investigation and experience of using ESTISOL™ 240 and COASOL™ for ice-core drilling, Annals of Glaciology, 55, 219-232, doi:10.3189/2014AoG68A036, 2014.

Steinbach, F., Bons, P. D., Griera, A., Jansen, D., Llorens, M.-G., Roessiger, J., and Weikusat, I.: Strain localization and dynamic recrystallization in teh ice-air aggregate: a numerical study. The Cryosphere, 10, 3071-3089, doi:10.5194/tc-10-3071-2016, 2016.

Steinbach, F., Kuiper, E. N., Eichler, J., Bons, P. D., Drury, M. R., Griera, A., Pennock, G., Weikusat, I.: The Relevance of Grain Dissection for Grain Size Reduction in Polar Ice: Insights from Numerical Models and Ice Core Microstructure Analysis. Frontiers in Earth Science, 5, 1-19, doi:10.3389/feart.2017.00066, 2017.

Suwa, M., von Fischer, J. C., Bender, M. L., Landais, A., and Brook, E. J.: Chronology reconstruction for the disturbed bottom section of the GISP2 and the GRIP ice cores: Implications for Termination II in Greenland. Journal of Geophysical Research, 111, 2, doi:10.1029/2005JD006032, 2006.

Thorsteinsson, T., Waddington, E. D., Taylor, K. C., Alley, R. B., and Blankenship, D. D.: Strain-rate enhancement at Dye 3, Greenland. Journal of Glaciology, 45, 338-345, doi:10.3189/002214399793377185, 1999.

Thorsteinsson, T., Kipfstuhl, J., Eicken, H., Johnsen, S. J., and Fuhrer, K.: Crystal size variations in Eemian-age ice from the GRIP ice core, Central Greenland. Earth and Planetary Science Letters, 131, 381-394, doi:10.1016/0012-821X(95)00031-7, 1995.

Thorsteinsson, T., Kipfstuhl, J., and Miller, H.: Textures and fabrics in the GRIP ice core. Journal of Geophysical Research, 102, 26583-26599, doi:10.1029/97JC00161, 1997.

Van de Wal, R. S. W., Boot, W., Van den Broeke, M. R., Smeets, C. J. P. P., Reijmer, C. H., Donker, J. J. A., and Oerlemans, J.: Large and Rapid Melt-Induced Velocity Changes in the Ablation Zone of the Greenland Ice Sheet, Science, 321, 111-113, doi:10.1126/science.1158540, 2008.

Van der Veen, C. J., and Whillans, I. M.: Development of fabrics in ice. Cold Regions Science and Technology, 22, 171-195, doi:10.1016/0165-232X(94)90027-2, 1994.

Von Mises, R.: Mechanik der Plastischen Formänderung von Kristallen. Zeitschrift für Angewandte Mathematik und Mechanik, 8, 161-185, 1928.

Weertman, J.: Creep deformation of ice. Annual Reviews of Earth and Planetary Sciences, 11, 215-240, 1983.

Weikusat, I., Jansen, D., Binder, T., Eichler, J., Faria, S. H., Wilhelms, F., Kipfstuhl, S., Sheldon, S., Miller, H., Dahl-Jensen, D., and Kleiner, T.: Physical analysis of an Antarctic ice core (EDML) – towards an integration of micro- and macrodynamics of polar ice. Philosophical Transactions A, 375, doi:10.1098/rsta.2015.0347, 2017.

Weikusat, I., and Kipfstuhl, S.: Crystal c-axes (fabric) of ice core samples collected from the NEEM ice core. PANGAEA, https://doi.pangaea.de/10.1594/PANGAEA.744004, 2010.

Wenk, H.-R., Canova, A., Molinari, A., and Kocks, U. F.: Viscoplastic modelling of texture development in quartzite. Journal of Geophysical Research, 94, 17895-17906, doi:10.1029/JB094iB12p17895, 1989.

Wettlaufer, J. S.: Ice Surfaces : Macroscopic Effects of Microscopic Structure. Philosophical Transactions: Mathematical, Physical and Engineering Sciences, 357, 3403-3425, 1999a.

Wettlaufer, J. S.: Impurity effects in the Premelting of Ice. Physical Review Letters, 82, 2516-2519, doi:10.1103/PhysRevLett.82.2516, 1999b.

Wilson, C. J. L., and Zhang, Y.: Development of microstructure in the high-temperature deformation of ice. Annals of Glaciology, 23, 293-302, doi:10.3189/S0260305500013562, 1996.

Wilson, C. J. L., Zhang, Y., and Stüwe, K.: The effects of localized deformation on melting processes in ice. Cold Regions Science and Technology, 24, 177-189, 1996.

Wolovick, M. J., and Creyts, T. T.: Overturned folds in ice sheets: Insights from a kinematic model of traveling sticky patches and comparisons with observations. Journal of Geophysical Research: Earth Surface, 121, 1065-1083, doi: 10.1002/2015JF003698, 2016.

Woodcock, N. H.: Specification of fabric shapes using an eigenvalue method. Journal of Structural Geology, 88, 1231-1236, doi:10.1130/0016-7606(1977)88<1231:SOFSUA>2.0.CO;2, 1977.

Zwally, H. J., Abdalati, W., Herring, T., Larson, K., Saba, J., and Steffen, K.: Surface Melt-Induced Acceleration of Greenland Ice-Sheet Flow. Science, 297, 218-223, doi:110.1126/science.1072708, 2002.

The Cryosphere Discuss., https://doi.org/10.5194/tc-2018-275
Manuscript under review for journal The Cryosphere
Discussion started: 20 February 2019

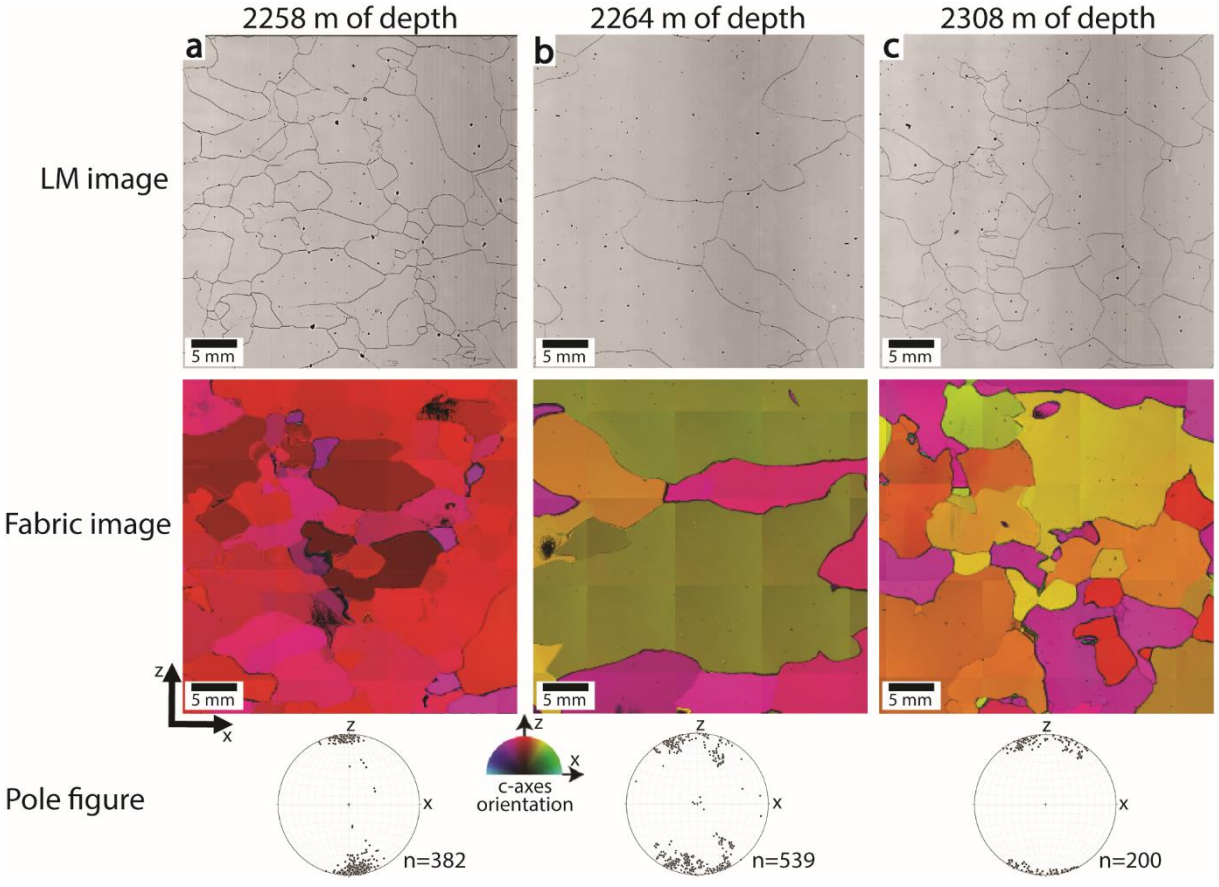

Figure 1: Part of vertical reflective LM images, orientation images and pole figures from three different ice core sections in the Eemian-glacial facies. The ice core sections in a) and b) are just above (2258 m of depth) and below (2264 m of depth) the stratigraphic disruption at 2262.2 m of depth, while c) is from the middle of one of the overturned layers (2308 m of depth). The z-axis Is parallel to the (vertical) ice core axis. The number of grains n included in the whole (90 x 55 mm) orientation image and pole figure is provided next to the pole figure (equal area, vertical plane, one point per grain). The pole figure in (b) contains the c-axes data from six consecutive ice core sections to increase the number of grains in the pole figure. LM images taken from Kipfstuhl (2010) (doi:10.1594/PANGAEA.743296). Fabric images and pole figures taken from Weikusat et al. (2010) (doi:10.1594/PANGAEA.744004).

The Cryosphere Discuss., https://doi.org/10.5194/tc-2018-275
Manuscript under review for journal The Cryosphere
Discussion started: 20 February 2019

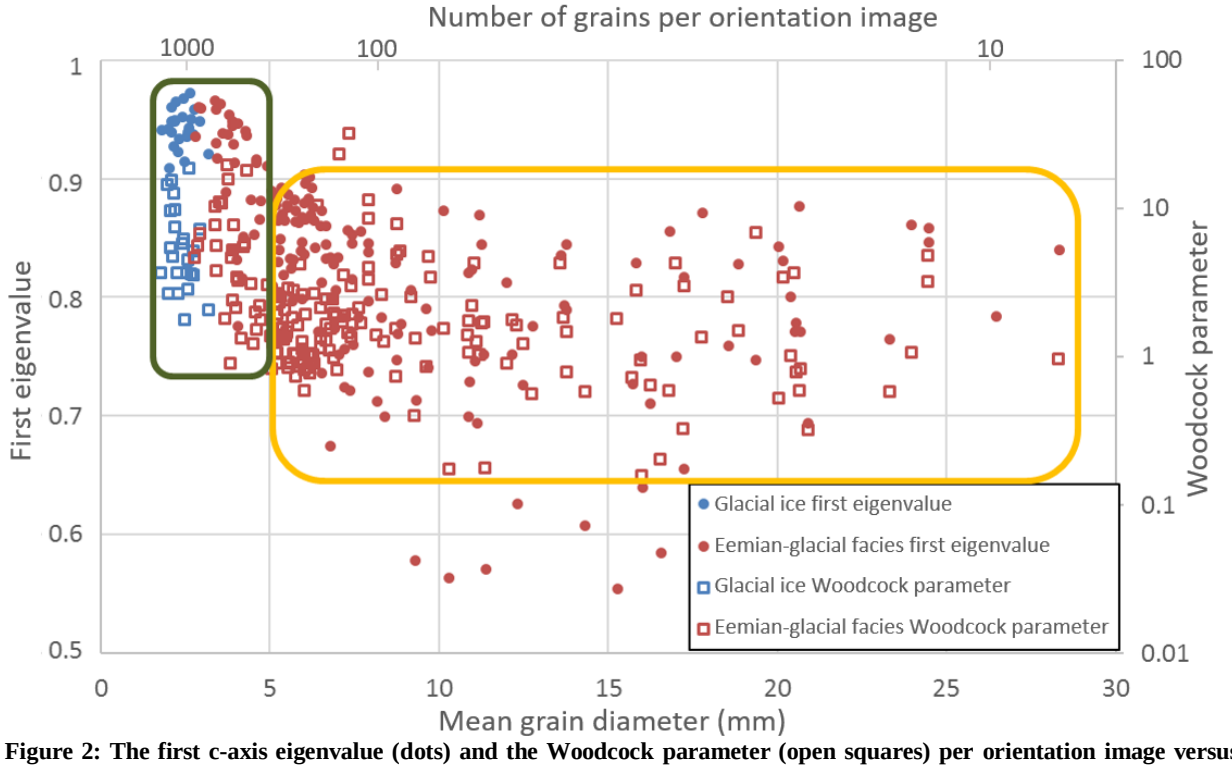

Figure 2: The first c-axis eigenvalue (dots) and the Woodcock parameter (open squares) per orientation image versus the mean grain diameter of the ice core sections in the lower part of the glacial ice (2000-2207 m of depth) in blue and the Eemian-glacial facies (2207-2540 m of depth) in red. The number of grains per orientation image was estimated by dividing the area of the orientation image by the mean grain area. The mean grain diameter was derived from orientation images, which gives a slightly lower mean grain diameter than the mean grain diameter derived using the Ice-image software. Two classes of grains can be distinguished based on mean grain diameter, eigenvalue and Woodcock parameter. One class (green rectangle) has a fine mean grain size <5 mm and an eigenvalue and Woodcock parameter that is comparable to the glacial ice and the other class (yellow rectangle) with a larger mean grain diameter (>5 mm) that has a lower eigenvalue and Woodcock parameter.

The Cryosphere Discuss., https://doi.org/10.5194/tc-2018-275
Manuscript under review for journal The Cryosphere
Discussion started: 20 February 2019

Table 1: Polar ice cores drilled at the Greenland and Antarctic ice sheets that show a sudden increase in grain size and change in CPO in the lower part of the ice core. The depth where these changes occur is given, together with ice core length, bottom borehole temperature, the in-situ temperature and the pressure-corrected temperature (T*) at the sudden grain size increase and change in CPO and the age of the ice at the transition to a sudden grain size increase and change in CPO. The age of the ice at the transition to a microstructure where temperatures are sufficient to cause premelting that would enhance GB mobility and enhance strain induced boundary migration (SIBM) is given in marine isotope stages (MIS) (Lisiecki and Raymo, 2005).

Name of ice core	Ice core length (m)	Borehole bottom T (°C)	Depth grain size increase and/or CPO change (m)	In-situ T at grain size increase and/or CPO change (°C)	Pressure-corrected temperature T* (°C)	Age of ice at transition to enhanced SIBM microstructure
Byrd[1]	2164	-1.6*	1810	-13	-11	MIS 3
EDC[2]	3270	-2.3*	2812	-13	-11	MIS 12
EDML[3]	2774	-3*	2370	-13	-11	MIS 6–MIS 5e
GISP2[4]	3053	-9	2950	-14	-11	MIS 6-MIS 5
GRIP[5]	3029	-9	2790	-13	-11	MIS 5e-MIS 5d
NEEM[6]	2540	-3.4	2207	-12	-10	MIS 5e-MIS 5d
Siple dome[7]	1004	-1.3	605	-13	-12	MIS 1
WAIS[8]	3405	unknown	3000	just below -10**	not applicable	MIS 3

***Subglacial water encountered during drilling close to the bedrock.**
****A specific temperature was not given, only that the grain size increase started just below -10°C.**
[1]Gow and Williamson (1976); Hammer et al. (1994); Gow and Engelhardt (2000); Epstein et al. (2011).
[2]EPICA community members (2004); Augustin et al. (2007); Durand et al. (2009).
[3]Ruth et al. (2007); Weikusat et al. (2017).
[4]Gow et al. (1997); Suwa et al. (2006).
[5]Johnsen et al. (1995); Thorsteinsson et al. (1997); Suwa et al. (2006).
[6]NEEM community members (2013); Sheldon et al. (2014).
[7]Nereson et al. (1996); Gow and Engelhardt (2000).
[8]Fitzpatrick et al. (2014); Buizert et al. (2015).

The Cryosphere Discuss., https://doi.org/10.5194/tc-2018-275
Manuscript under review for journal The Cryosphere
Discussion started: 20 February 2019

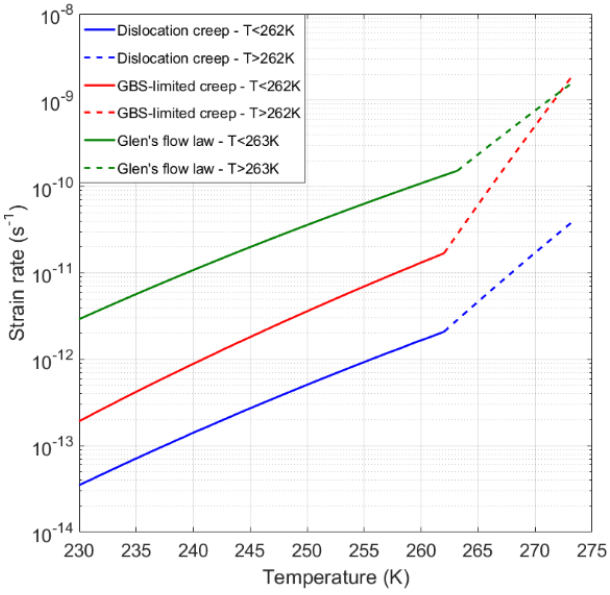

Figure 3: Log strain rate versus temperature for Glen's flow law and the two mechanisms (dislocation creep and GBS-limited creep) that form the end members of the modified composite flow law, using the flow law parameters from Table 2. A stress of 0.07 MPa and a mean grain diameter of 5 mm were used to calculate the strain rate.

Table 2: The flow law parameters of Glen's flow law (Paterson, 1994) and the end members of the modified composite flow law for dislocation creep and GBS-limited creep.

Creep regime	A (units)	n	p	Q (kJ mol^{-1})
Glen's flow law (T<263K)	$3.61\ 10^{5} MPa^{-3.0} s^{-1}$	3.0	0	60
Glen's flow law (T>263K)	$1.73\ 10^{21} MPa^{-3.0} s^{-1}$	3.0	0	139
Dislocation creep (T<262K)	$5.0\ 10^{5} MPa^{-4.0} s^{-1}$	4.0	0	64
Dislocation creep (T>262K)	$6.96\ 10^{23} MPa^{-4.0} s^{-1}$	4.0	0	155
GBS-limited creep (T<262K)	$1.1\ 10^{2} MPa^{-1.8} m^{1.4} s^{-1}$	1.8	1.4	70
GBS-limited creep (T>262K)	$8.5\ 10^{37} MPa^{-1.8} m^{1.4} s^{-1}$	1.8	1.4	250

The Cryosphere Discuss., https://doi.org/10.5194/tc-2018-275
Manuscript under review for journal The Cryosphere
Discussion started: 20 February 2019

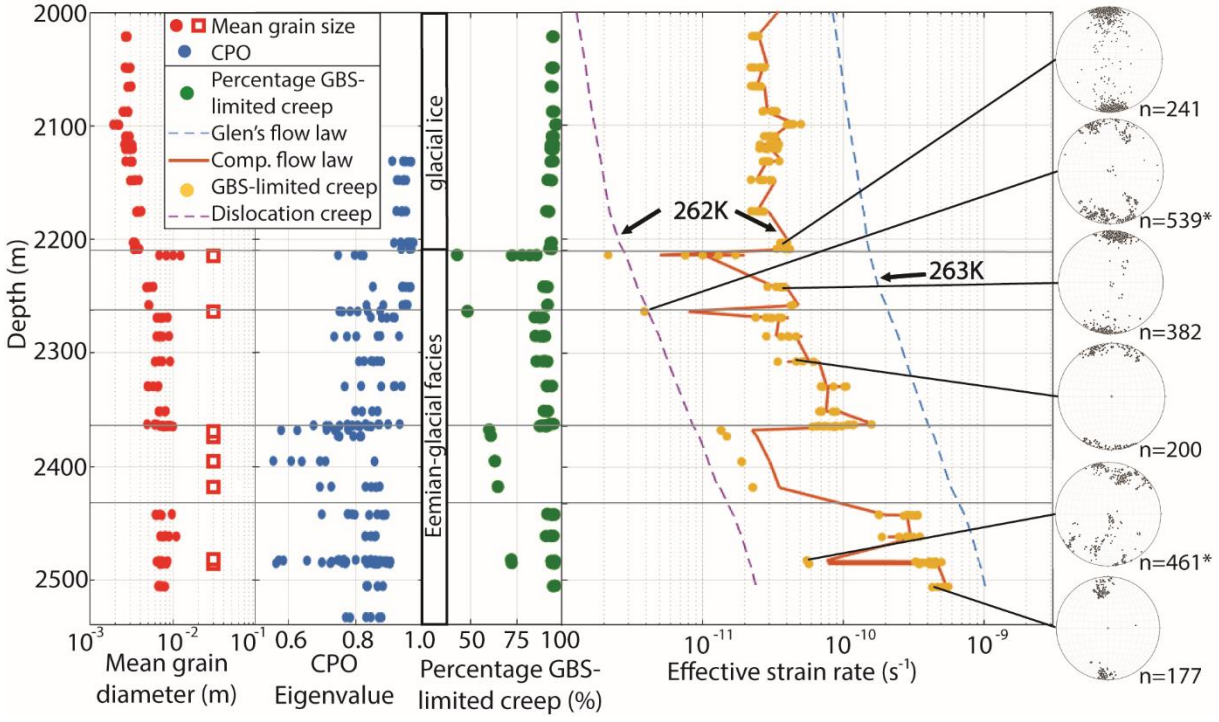

Figure 4: Results showing as a function of depth for the lowest 540 m of the NEEM ice core, the mean grain diameter (red dots), first CPO eigenvalues (blue dots), calculated strain rates (Table 2) using Glen's flow law (blue dotted line), the modified composite flow law (orange line) and the two end-member deformation mechanisms, dislocation creep (purple dotted line) and GBS-limited creep (yellow dots), (where, the orange line shows the total strain rates smade up of the dislocation creep strain rate, shown by the purple line and the GBS-limited strain rate, shown by the yellow dots). The percentage contribution of GBS-limited creep to bulk strain rate is also shown (green dots). A red open square instead of a red dots was used when the grains size was too large to determine a mean grain diameter by the Ice-image software and a mean grain diameter of 30 mm was used. The four horizontal grey lines represent the stratigraphic disruptions that were found in the NEEM deep ice core (NEEM community members, 2013). The glacial ice extends to a depth of 2207 m, with the glacial-Eemian facies continuing until the ice-bedrock interface at 2540 m depth. The depth of the temperature (T*) threshold for the modified composite flow law (262K) and Glen's flow law (263K) are indicated. On the right, six pole figures (equal area, vertical plane, one point per grain) at different depths are shown with the number of grains (*n*) next to the pole figure. At two depths, indicated by an asterisk (*), the CPO data from six consecutive ice core sections were combined to increase the number of grains in the pole figure. Pole figures in last panel taken from Weikusat et al. (2010) (doi:10.1594/PANGAEA.744004).